Acta Pharmacologica Sinica

www.nature.com/aps

ARTICLE

Par3L, a polarity protein, promotes M1 macrophage polarization and aggravates atherosclerosis in mice via p65 and ERK activation

Yi-min Huang[1], Yu-sen Wu[1], Yuan-ye Dang[1], Yi-ming Xu[2], Kong-yang Ma[3] and Xiao-yan Dai[1]✉

Proinflammatory M1 macrophages are critical for the progression of atherosclerosis. The Par3-like protein (Par3L) is a homolog of the Par3 family involved in cell polarity establishment. Par3L has been shown to maintain the stemness of mammary stem cells and promote the survival of colorectal cancer cells. In this study, we investigated the roles of the polar protein Par3L in M1 macrophage polarization and atherosclerosis. To induce atherosclerosis, *Apoe*$^{-/-}$ mice were fed with an atherosclerotic Western diet for 8 or 16 weeks. We showed that Par3L expression was significantly increased in human and mouse atherosclerotic plaques. In primary mouse macrophages, oxidized low-density lipoprotein (oxLDL, 50 μg/mL) time-dependently increased Par3L expression. In *Apoe*$^{-/-}$ mice, adenovirus-mediated Par3L overexpression aggravated atherosclerotic plaque formation accompanied by increased M1 macrophages in atherosclerotic plaques and bone marrow. In mouse bone marrow-derived macrophages (BMDMs) or peritoneal macrophages (PMs), we revealed that Par3L overexpression promoted LPS and IFNγ-induced M1 macrophage polarization by activating p65 and extracellular signal-regulated kinase (ERK) rather than p38 and JNK signaling. Our results uncover a previously unidentified role for the polarity protein Par3L in aggravating atherosclerosis and favoring M1 macrophage polarization, suggesting that Par3L may serve as a potential therapeutic target for atherosclerosis.

Keywords: atherosclerosis; aorta; macrophage polarization; Par3L; p65; ERK

Acta Pharmacologica Sinica (2023) 0:1–13; https://doi.org/10.1038/s41401-023-01161-z

INTRODUCTION

With the prevalence of unhealthy lifestyles, increased stress, and aging, atherosclerotic cardiovascular disease (ASCVD) has globally become the leading cause of morbidity and mortality [1]. Atherosclerosis is a chronic vascular inflammatory condition mainly characterized by lipid-driven arterial intimal damage. Risk factors, such as hypertension, hyperlipidemia, obesity, and diabetes, contribute to endothelial injury and lipid accumulation in the sub-intimal space [2, 3]. These lipid deposits, in turn, activate the immuno-inflammatory responses, leading to the transmigration of innate and adaptive immune cells into the subintimal area, facilitating the formation of atherosclerotic plaques [4]. Many kinds of immune cells are involved in the pathophysiology of atherosclerosis, including monocytes/macrophages, smooth muscle cells, endothelial cells, mast cells, eosinophils, dendritic cells, T cells, and B cells [5]. However, macrophages play essential roles in the whole process of the initiation and progression of atherosclerosis.

In atherosclerotic lesions, macrophages have dynamic plasticity and diversity [6]. They can differentiate into multiple functional phenotypes in response to various microenvironmental stimuli, such as oxidized lipids, cytokines, and cholesterol [6]. Macrophages have two major polarized phenotypes, namely classically activated macrophages (M1) and alternatively activated macrophages (M2) [6–8]. Pro-inflammatory transcription factors are upregulated, and mitogen-activated protein kinase (MAPK) or other inflammation-related signaling pathways are activated in M1 macrophages [9–12]. Eventually, M1 macrophages secrete pro-inflammatory cytokines, including interleukin (IL)-6, IL-1β, TNF-α, iNOS, IL-12, and IL-23, instigating inflammation [6, 13, 14]. Increasing animal studies have shown that inhibiting M1 macrophage polarization attenuates atherosclerosis [15–18]. Taken together, inhibiting M1 macrophage polarization may represent a novel strategy to protect against ASCVD.

Cell polarity is defined as the interactions between polar protein complexes that cause asymmetrical distribution of the plasma membrane, cytoskeleton, organelles, or biomacromolecules. Cell polarity plays a crucial role in the asymmetric division, development, differentiation, and proliferation of cells. The Par3-like protein (Par3L), also known as Pard3B, Par3B, or Par3β, is a novel homolog of the Par3 family involved in cell polarity establishment, with N-terminal fragments localized at tight junctions and colocalized with zonula occludens-1 (ZO-1) [19, 20]. It has been reported that the Ser746 phosphorylation site of Par3L interacts with 14-3-3 proteins [21]. Recent studies have shown that Par3L overlays with E-cadherin and Src at the adhesion junction of

[1]Key Laboratory of Molecular Target & Clinical Pharmacology and the State Key Laboratory of Respiratory Disease, School of Pharmaceutical Sciences, Guangzhou Medical University, Guangzhou 511436, China; [2]School of Basic Medical Sciences, Guangzhou Medical University, Guangzhou 511436, China and [3]Centre for Infection and Immunity Studies (CIIS), School of Medicine, Sun Yat-sen University, Shenzhen 518107, China
Correspondence: Xiao-yan Dai (xdai@gzhmu.edu.cn)

Received: 13 April 2023 Accepted: 29 August 2023
Published online: 20 September 2023

monolayer epithelial cells and may be involved in the E-cadherin-Src signaling pathway [22]. Previous studies have shown that Par3L plays a vital role in the maintenance of mammary stem cells by inhibiting liver kinase B1 (Lkb1) kinase activity [23]. Importantly, Par3L promotes the survival of colorectal cancer cells (CRC) by downregulating the Lkb1/AMP-activated protein kinase (AMPK) signaling pathway [24]. However, whether and how the polar protein Par3L affects atherosclerosis remains unknown.

In this work, we found that Par3L expression was increased in human and mouse atherosclerotic lesions, especially in macrophages. In addition, Par3L was increased in oxLDL-treated mouse primary macrophages. In vivo, we illustrated that adenovirus-mediated Par3L overexpression aggravated atherosclerosis in *Apoe*$^{-/-}$ mice by increasing non-high-density lipoprotein cholesterol (non-HDL-C), decreasing high-density lipoprotein cholesterol (HDL-C), and modulating M1 macrophage polarization. Mechanistically, Par3L induces M1 macrophage polarization by activating p65 and extracellular signal-regulated kinase (ERK) signaling pathways. Notably, nuclear factor κB (NF-κB) inhibitor Bay 11-7082 or ERK inhibitor PD98059 antagonized the accelerated effect of Par3L on M1 macrophage polarization. Here, we demonstrated a previously undefined pro-atherosclerotic and M1 macrophage-switching effect of Par3L.

MATERIALS AND METHODS

Human study

Atherosclerotic plaque specimens were obtained from patients who underwent carotid endarterectomy at Nanfang Hospital, Southern Medical University. Normal carotid arteries were acquired from individuals who had passed away due to a road traffic accident but had no history of cardiovascular diseases. The study procedures received ethical approval from the Institutional Review Board of Nanfang Hospital (approval number: 02800), Southern Medical University. Participants or their relatives provided informed consent by signing consent forms. All collected tissue samples were rapidly frozen using liquid nitrogen before being subjected to analysis.

Experimental animals

The experimental protocols were approved by the Animal Research Ethics Committees of Guangzhou Medical University (permit number: 2019-016). *Apoe*$^{-/-}$ mice were purchased from Shanghai Model Organisms (Shanghai, China). The custom-made adenovirus with full-length cDNA of human Par3L (Ad-hPar3L) was purchased from Vigene Biological Technology Company (Ji-nan, China). Ad-GFP was used as a control. Eight-week-old male *Apoe*$^{-/-}$ mice were injected with Ad-GFP or Ad-hPar3L through tail vein once every 4 weeks at a dose of 2×10^{10} U. The Western diet irradiated with cobalt-60 (containing 21% fat, 0.15% cholesterol, and 15.5% protein) was purchased from Guangdong Medical Laboratory Animal Center (Foshan, China). All mice were fed a Western diet for 12 weeks, had free access to food and water, and were maintained in the Experimental Animal Center of Guangzhou Medical University under specific-pathogen-free (SPF) conditions. All mice were performed in accordance with the National Institutes of Health (NIH) Guide for the Care and Use of Laboratory Animals.

Cell culture and treatment

Eight-week-old male C57BL/6J mice were purchased from Shanghai Model Organisms (Shanghai, China). Mouse primary bone marrow-derived macrophages (BMDMs) and peritoneal macrophages (PMs) were isolated from 8-week-old male C57BL/6J mice, as previously described [25–27]. After extraction from C57BL/6J mice, BMDMs were cultured in RPMI-1640 medium (EH80809, Cytiva) supplemented with 10% fetal bovine serum (FBS, 10270106, Gibco), 1% penicillin/streptomycin (PS, 15140122, Gibco) and 25 ng/mL macrophage colony-stimulating factor (M-CSF, 14-8983-80, eBioscience) for 6 days at 37 °C to differentiate into mature macrophages (M0-phenotype). M0 macrophages were then infected with Ad-GFP and Ad-hPar3L in RPMI-1640 complete medium for 8 h at 37 °C and continued culture for 24 h after replacing fresh medium, and polarized into M1 macrophages by stimulation with 100 ng/mL LPS (tlrl-smlps, InvivoGen) and 20 ng/mL IFNγ (RP-8617, InvivoGen) for additional 24 h.

Eight-week-old male C57BL/6J mice were injected intraperitoneally with 1.5 mL 4% sterile thioglycollate broth (211716, BD Biosciences) for 3 days. PMs were extracted and cultured in RPMI-1640 medium containing 10% FBS, 1% PS for 12 h at 37 °C, and then infected with Ad-GFP and Ad-hPar3L in RPMI-1640 complete medium for 8 h at 37 °C, and continued culture for 24 h after replacing fresh medium, and polarized into M1 macrophages by stimulation with 100 ng/mL LPS and 20 ng/mL IFNγ for another 24 h.

Quantification of atherosclerotic lesions

For the lesions in the *en face* aortas, *en face* aortas were carefully and rapidly separated after removing excess adipose tissue using a stereomicroscope and fixed in 4% PFA for at least 24 h. Afterward, *en face* aortas were washed with PBS, 60% isopropanol was used to balance blood vessels, and stained with 0.5% Oil Red O (O0625, Sigma-Aldrich) at 37 °C for 1 h. Next, *en face* aortas were destained with 60% isopropanol for 10 s and rewashed. The aortas were opened longitudinally at the thoracic aorta and aortic arch and spread flat on a 10 cm black wax dish, fixed with capillary needles (26002-10, FST), as previously described [28]. The images were captured using a camera (750D, Canon), and the percent total aortic area occupied by *en face* Oil Red O-stained lesions was analyzed using ImageJ.

For the lesions at the aortic roots, the heart from mice cut transversely was fixed in 4% PFA at 4 °C for 12 h, dehydrated with 30% sucrose (57-50-1, DM) and then embedded in OCT compound (1402010892, Leica) for further experiments. The aortic root sections were serially cut with a Leica (Leica Biosystems, Wetzlar, Germany) at 6 μm. Slides were stained with 0.5% Oil Red O, hematoxylin-eosin (H&E, C0105, Beyotime), and Masson's trichrome (G1346, Solarbio) according to the manufacturer's protocol. Finally, seal the slides with 90% glycerin or resin. Plaque images were obtained using an Aperio Digital Pathology Slide Scanner (Leica CS2, CA, USA) and quantitatively analyzed using ImageJ. The calculation formula was as follows: (macrophage staining % + lipid staining %)/(α-SMA staining % + collagen fiber staining %), as described previously [28–31].

Immunofluorescence (IF)

Slides were fixed in 4% PFA for 30 min, washed with PBS, blocked with 0.3% Triton X-100 (V900502, Sigma-Aldrich), 10% Western blocking reagent (WBR, 11921673001, Roche), and 5% goat serum (SL038, Solarbio) in PBS for 1 h at room temperature, and then incubated with primary antibodies overnight at 4 °C. Slides were rinsed with PBS and incubated with secondary antibodies for 1 h at room temperature in the dark. The nuclei were marked blue using 4′,6-diamidino-2-phenylindole (DAPI, D1306, Invitrogen). All primary and secondary antibodies used for immunofluorescence staining are listed in Supplementary Table S1. Slides were mounted and visualized using a Nikon A1R laser confocal microscope (Tokyo, Japan).

Flow cytometry

The mice were euthanized, followed by cardiac puncture to take blood samples, and then placed in a 5 mL anticoagulant tube containing heparin sodium (SY-733, SANLI). Mice were subjected to cardiac perfusion with sterile PBS. As previously described, we obtained single-cell suspensions of the spleen and bone marrow and performed flow cytometry staining of cell membranes [28]. All

antibodies used for flow cytometry are listed in Supplementary Table S1. All samples were immediately acquired on a BD LSR Fortessa cytometer (CA, USA) after staining and analyzed using FlowJo software (BD Biosciences, CA, USA).

Plasma lipid examination

Plasma was prepared to determine the lipid levels of total cholesterol (TC), triglycerides (TG), non-HDL-C, and HDL-C by a Hitachi 7600 automatic biochemical analysis instrument (Hitachi, Japan).

Protein extract and Western blot analysis

In this study, Western blot experimental procedure and analysis were performed as previously described [32]. Briefly, total protein from BMDMs or PMs was lysed with RIPA buffer (FD008, Fdbio Science) containing a protease inhibitor cocktail (HY-K0010, MedChemExpress). Protein concentrations were determined using the bicinchoninic acid (BCA) protein assay (P0009, Beyotime). Thirty micrograms of protein samples were resolved by 10% or 12% sodium dodecyl sulfate-polyacrylamide gel electrophoresis (SDS-PAGE). After transferring the proteins to the 0.22 μm nitrocellulose membrane (66485, PALL), the membrane was blocked in 5% skimmed milk (232100, BD) or 5% BSA (V900933, Sigma-Aldrich) for 1 h at room temperature, and then incubated with the primary antibodies at 4 °C overnight on a shaker. All antibodies used for Western blotting are shown in Supplementary Table S1. The membranes were washed and incubated successively with HRP-conjugated secondary antibodies and visualized with Chemiluminescent HRP Substrate the next day (WBKLS0500, Millipore). Protein bands were obtained through Amersham Imager 680 (GE Healthcare, Chicago, IL, USA) and quantified using ImageJ. GAPDH or β-actin was used as an internal control.

RNA extractions and real-time quantitative PCR (qPCR)

Total RNA from BMDMs, PMs, or liver samples was extracted using TRIzol reagent (21101, Accurate Biology, Changsha, China). cDNA synthesis was performed using a reverse transcription kit (11706, AG). Next, qPCR was conducted with an SYBR green real-time PCR premix kit (11701, AG) on a Light Cycler® 480 Instrument II (Roche, Basel, Switzerland). All primers were synthesized by Beijing Qingke Biotech Technology Company, and sequences are listed in Supplementary Table S2. The $2^{-\Delta\Delta Ct}$ method was used to compare and calculate the relative quantitative values. GAPDH as a normalized internal reference gene for qPCR.

Statistical analysis

All statistical analysis was performed using GraphPad Prism version 8. Data are presented as mean ± SEM. An unpaired, two-tailed Student's *t*-test was used to compare 2 groups. NS, not significant. Statistical significance is indicated as follows: $^{*}P < 0.05$, $^{**}P < 0.01$, $^{***}P < 0.001$, and $^{****}P < 0.0001$.

RESULTS

The expression of Par3L is increased in human and mouse atherosclerotic plaques

To explore the potential involvement of Par3L in the pathogenesis of atherosclerosis, we first determined the Par3L expression in human normal carotid arteries and carotid atherosclerotic plaques. Immunofluorescence staining showed that Par3L expression is higher in human carotid atherosclerotic plaques than in normal arteries (Fig. 1a). We also examined the expression of Par3L in *Apoe*$^{-/-}$ mice fed with a normal chow or an atherosclerotic Western diet for 8 or 16 weeks. As shown in Fig. 1b, c, immunofluorescence staining of Par3L and F4/80 revealed that a great number of macrophages accumulated in atherosclerotic lesions after 8 and 16 weeks of Western diet feeding. Strikingly, Par3L was dramatically increased in atherosclerotic lesion areas upon Western diet feeding, especially in macrophages (Fig. 1b, c). Taken together, these data suggest that Par3L expression is significantly upregulated in human and mouse atherosclerotic plaques, implying a potential involvement of Par3L in atherosclerosis development.

Atherosclerotic risk factor oxLDL upregulates Par3L in primary mouse macrophages

OxLDL is a well-known risk factor for atherosclerosis. To observe whether oxLDL affects Par3L expression in macrophages, we treated BMDMs and PMs with 50 μg/mL oxLDL. As shown in Fig. 2a, b, Par3L protein levels were induced by oxLDL in a time-dependent manner in BMDMs and PMs. Furthermore, immunofluorescence staining confirmed higher Par3L protein expression in oxLDL-treated BMDMs and PMs (Fig. 2c, d). We also examined the effect of oxLDL on the mRNA expression of Par3L. qPCR analysis demonstrated that the mRNA expression of Par3L did not exhibit a significant change in response to oxLDL treatment in both BMDMs and PMs at 0, 12, or 24 h (Supplementary Fig. S1a, b). Together, Par3L is increased in primary mouse BMDMs and PMs incubated with oxLDL.

Adenovirus-mediated Par3L overexpression aggravates atherosclerosis in *Apoe*$^{-/-}$ mice in vivo

To directly evaluate the effects of Par3L on atherosclerosis development in mice, *Apoe*$^{-/-}$ mice were injected with Ad-GFP or Ad-hPar3L adenovirus via the lateral tail vein, followed by a 12-week Western diet feeding (Fig. 3a). Par3L overexpression exhibited markedly increased atherosclerosis lesion area in the aortas compared with Ad-GFP *Apoe*$^{-/-}$ mice (Fig. 3b, c). Consistently, Oil Red O and H&E staining of the aortic root also showed a significant increase in the lesion area in Par3L overexpression compared to Ad-GFP *Apoe*$^{-/-}$ mice (Fig. 3d, e). However, no significant difference was observed in collagen content (Fig. 3f). Notably, Par3L overexpression substantially increased the macrophage accumulation, as evidenced by immunofluorescence staining of macrophage marker F4/80 (Fig. 3g). In contrast, the content of smooth muscle cells showed no difference between the two groups, as suggested by immunofluorescence staining of smooth muscle cell marker α-SMA (Fig. 3h). Consequently, the vulnerability index of the plaque demonstrated that Par3L overexpression *Apoe*$^{-/-}$ mice had an increased plaque instability compared with Ad-GFP *Apoe*$^{-/-}$ mice (Fig. 3i). Collectively, these data suggest that Par3L accelerates atherosclerotic plaque formation in *Apoe*$^{-/-}$ mice in vivo.

Adenovirus-mediated Par3L overexpression increases non-HDL-C and decreases HDL-C levels in plasma

Dyslipidemia is a crucial factor leading to atherosclerosis and an independent risk factor for coronary heart disease and cerebrovascular disease [33]. For example, high non-HDL-C contributes to the development and progression of atherosclerosis [34]. In contrast, high HDL-C confers cardiovascular protection [35]. We next asked whether Par3L affects the blood lipid levels of *Apoe*$^{-/-}$ mice. As shown in Supplementary Fig. S2a, b, no significant difference in body weight or heart weight to body weight ratio (HW/BW) was found between Ad-GFP and Ad-hPar3L in *Apoe*$^{-/-}$ mice. Lipid profiling assay showed no significant difference between the two groups observed in plasma TG and TC levels (Supplementary Fig. S2c). However, higher non-HDL-C and lower HDL-C were detected in the plasma of Par3L overexpression *Apoe*$^{-/-}$ mice (Supplementary Fig. S2c). Given the dominant roles of the liver in lipid metabolism [36–38], we next determined the mRNA levels of genes involved in lipid metabolism in the liver. qPCR analysis showed that Ad-hPar3L increased the expression of *CCAAT/enhancer binding protein alpha* (*Cebpa*), a transcription factor critical for lipid synthesis, in the liver of *Apoe*$^{-/-}$ mice compared to the Ad-GFP (Supplementary Fig. S3). However, no

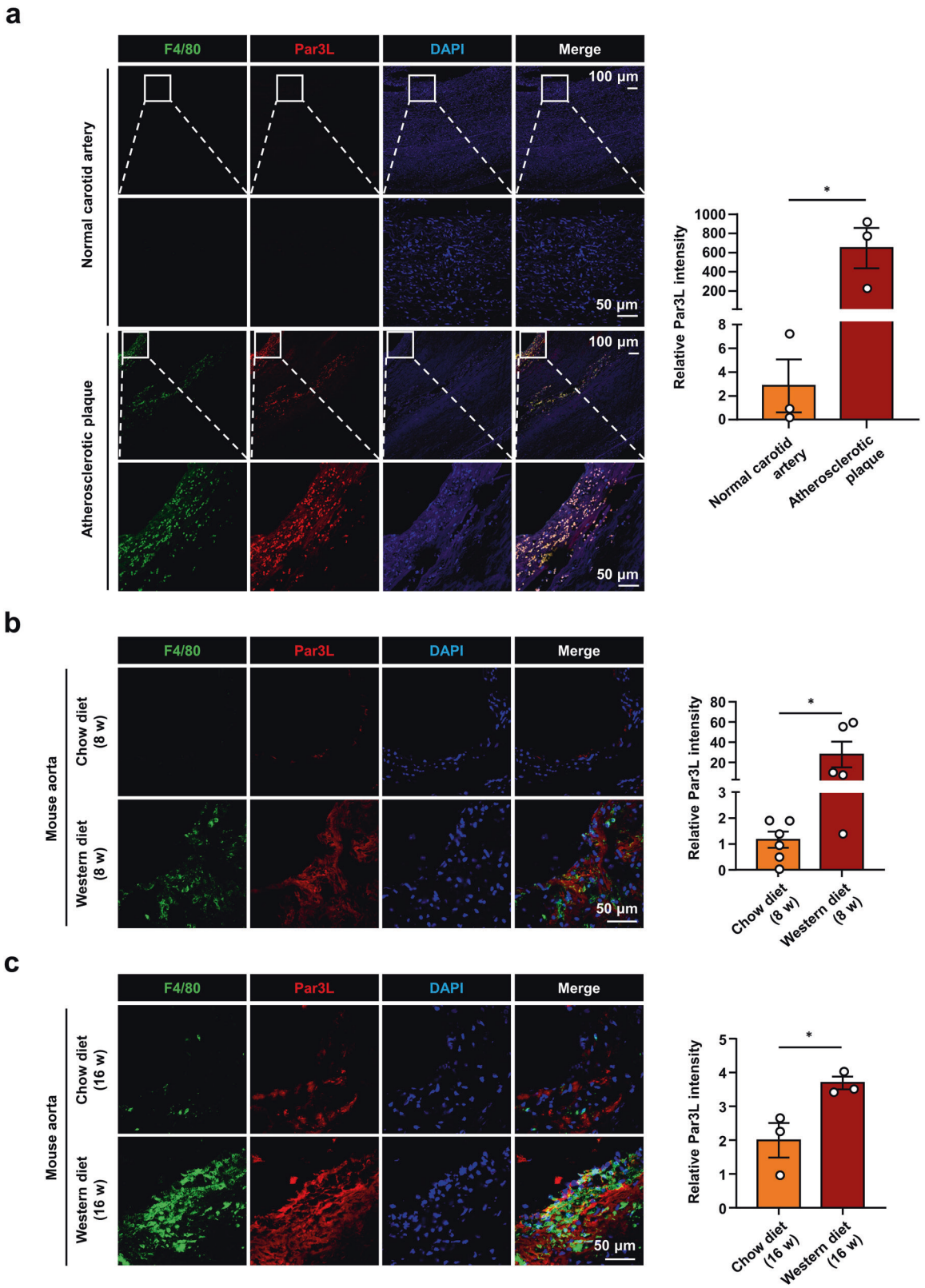

Fig. 1 The expression of Par3L is increased in human and mouse atherosclerotic plaques. a Representative immunofluorescence staining for F4/80$^+$ (green) and Par3L$^+$ (red) in human normal carotid arteries and atherosclerotic carotid artery (Atherosclerotic plaque) ($n = 3$ samples). Nuclei were labeled with DAPI (blue). Scale bar = 50 or 100 μm. **b** Representative immunofluorescence staining for F4/80$^+$ (green) and Par3L$^+$ (red) in aortic root lesions in *Apoe*$^{-/-}$ mice fed a chow diet or Western diet for 8 weeks ($n = 5$ or 6 mice). Nuclei were labeled with DAPI (blue). Scale bar = 50 μm. **c** Representative immunofluorescence staining for F4/80$^+$ (green) and Par3L$^+$ (red) in aortic root lesions in *Apoe*$^{-/-}$ mice fed a chow diet or Western diet for 16 weeks ($n = 3$ mice). Nuclei were labeled with DAPI (blue). Scale bar = 50 μm. Data are presented as mean ± SEM. *P* values were determined using unpaired, two-tailed Student's *t*-test. *$P < 0.05$, significantly different as indicated.

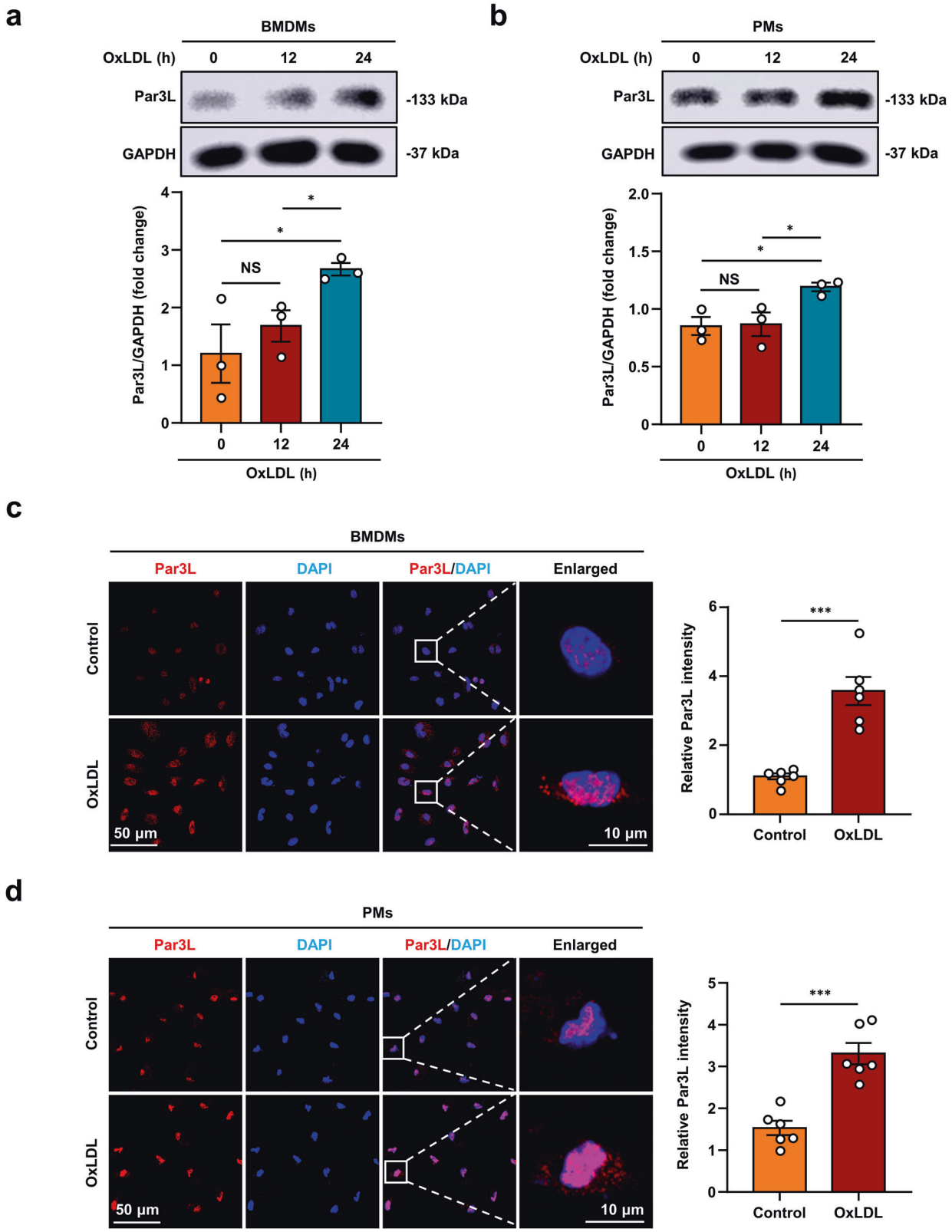

Fig. 2 Atherosclerotic risk factor oxidized low-density lipoprotein (oxLDL) upregulates Par3L in primary mouse macrophages. Representative immunoblots and quantification of Par3L protein levels in bone marrow-derived macrophages (BMDMs, **a**) or peritoneal macrophages (PMs, **b**) treated with 50 μg/mL oxLDL for 0, 12, or 24 h ($n = 3$). Immunofluorescence analysis of Par3L expression in BMDMs (**c**) or PMs (**d**) treated with or without 50 μg/mL oxLDL for 24 h ($n = 6$). Scale bar = 10 or 50 μm. Data are presented as mean ± SEM. *P* values were determined using unpaired, two-tailed Student's *t*-test. NS not significant. $^*P < 0.05$, $^{***}P < 0.001$, significantly different as indicated.

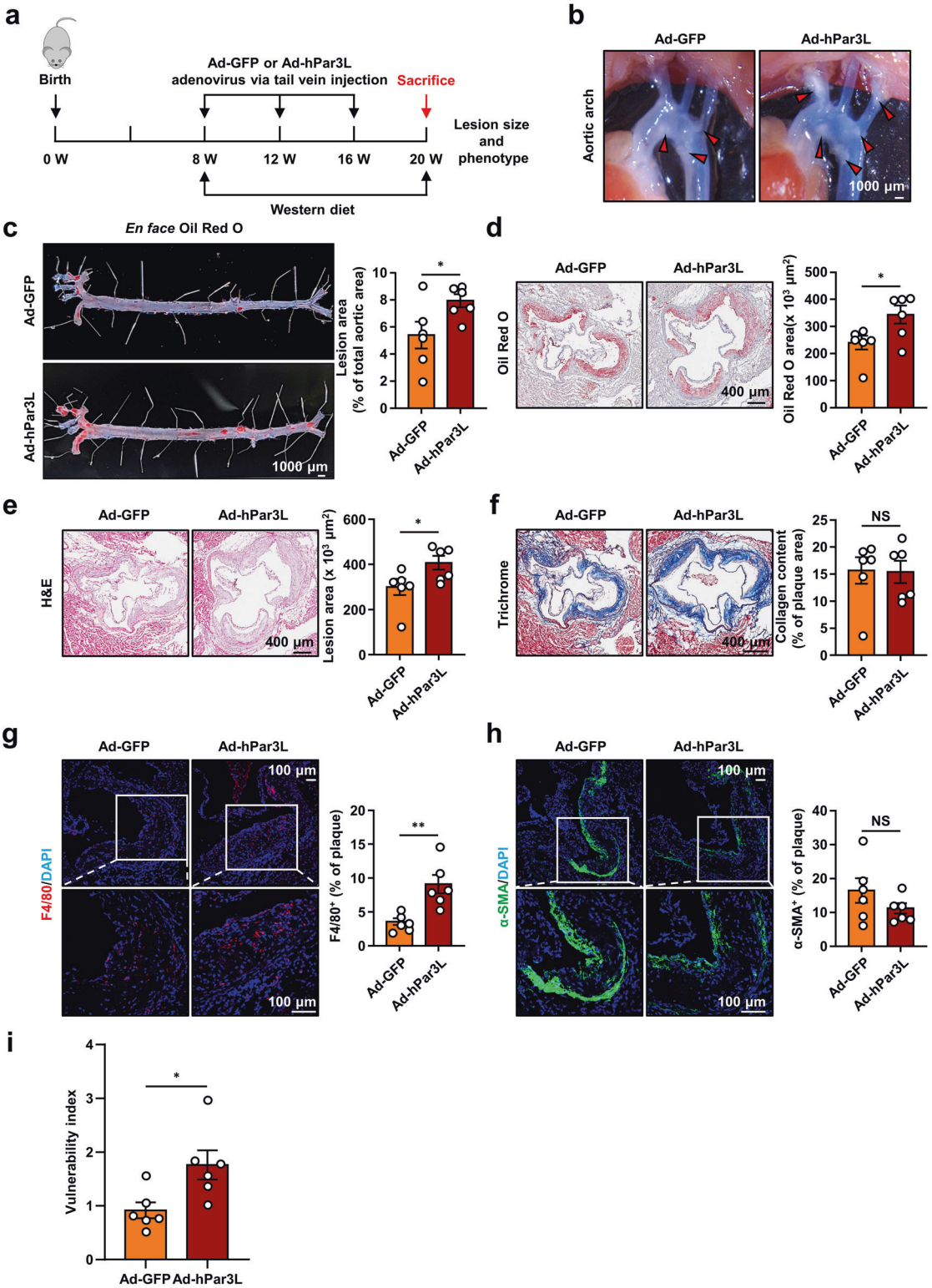

Fig. 3 Adenovirus-mediated Par3L overexpression aggravates atherosclerosis in *Apoe*$^{-/-}$ mice. a Experimental scheme showing that eight-week-old male *Apoe*$^{-/-}$ mice were injected with Ad-GFP or Ad-hPar3L through tail vein once every 4 weeks and fed a Western diet for 12 weeks. **b** Stereomicroscope was used to identify plaques (red arrows) in the aortic arches and thoracic aorta of *Apoe*$^{-/-}$ mice. Scale bar = 1000 μm. **c** Representative Oil Red O-stained *en face* aortas ($n = 6$ mice). Scale bar = 1000 μm. **d** Representative Oil Red O staining of aortic root sections ($n = 6$ mice). Scale bar = 400 μm. **e** Representative H&E staining of aortic root sections ($n = 6$ mice). Scale bar = 400 μm. **f** Representative Masson's trichrome staining of aortic root sections ($n = 6$ mice). Scale bar = 400 μm. **g, h** Representative F4/80 and α-smooth muscle actin (α-SMA) immunofluorescent staining of aortic root sections ($n = 6$ mice). Scale bar = 100 μm. F4/80$^+$ and α-SMA$^+$ areas were quantified as the percentages of the entire plaque area using ImageJ. **i** Vulnerability index of plaques ($n = 6$ mice). The calculation formula was as follows: (macrophage staining% + lipid staining%)/(α-SMA staining% + collagen fiber staining%). Data are presented as mean ± SEM. *P* values were determined using unpaired, two-tailed Student's *t*-test. NS not significant. **P* < 0.05, ***P* < 0.01, significantly different as indicated.

significant difference was observed in the mRNA levels of *Pparg*, *Atgl*, *Fabp4*, *Lpl*, *Fasn*, *Srebp-1c*, and *Accb*. In sum, these data suggest that Par3L increases non-HDL-C and decreases HDL-C levels in plasma, likely through upregulating *Cebpa* expression.

Adenovirus-mediated Par3L overexpression regulates M1 macrophage polarization in *Apoe*$^{-/-}$ mice in vivo

Macrophages are actively involved in the pathogenesis of atherosclerosis [4]. Classically activated M1 macrophages are involved in provoking and sustaining inflammation, whereas alternatively activated M2 macrophages are associated with resolving inflammation [4]. We assessed the proportion of M1 to M2 macrophages in the bone marrow, peripheral blood, and spleen collected from Ad-GFP and Ad-hPar3L in *Apoe*$^{-/-}$ mice using flow cytometry. The results demonstrated that Par3L did not significantly affect the proportion of M1 and M2 macrophages in the bone marrow, peripheral blood, and spleen (Fig. 4a). However, Par3L notably increased the ratio of M1 to M2 macrophages, indicating the involvement of Par3L in M1 macrophage polarization (Fig. 4a). To detect M1 macrophages in atherosclerotic plaques, we performed immunofluorescence analysis of F4/80 and ArgII. The results demonstrated that more M1 macrophages accumulate in the atherosclerotic lesions of Ad-hPar3L relative to Ad-GFP *Apoe*$^{-/-}$ mice (Fig. 4b). Thus, these data suggest that Par3L promotes M1 macrophage polarization in *Apoe*$^{-/-}$ mice in vivo.

Par3L promotes LPS and IFNγ-induced M1 macrophage polarization in vitro

To evaluate the role of Par3L in M1 macrophage polarization in vitro, we infected BMDMs or PMs with Ad-GFP or Ad-hPar3L adenovirus in the presence or absence of LPS and IFNγ. As shown in Fig. 5a, b, Western blot analysis showed that Par3L overexpression significantly increased the protein expression levels of iNOS, ArgII, pro-IL-1β, and cleaved IL-1β in BMDMs in the presence of LPS and IFNγ. Moreover, we also observed consistent results in PMs by Western blot analysis (Fig. 5c, d). Using qPCR analyses, we found that Par3L overexpression enhanced the mRNA levels of *Il-6*, *Il-1β*, and *Arg2* in PMs (Fig. 5e). Eventually, immunofluorescence staining demonstrated Par3L overexpression upregulated iNOS expression in both BMDMs and PMs (Fig. 5f, g). Conversely, Western blotting revealed that Par3L knockdown by siRNA significantly reduced the protein levels of iNOS and ArgII in BMDMs when treated with LPS and IFNγ (Supplementary Fig. S4a, b). Furthermore, immunofluorescence staining demonstrated that Par3L knockdown remarkably attenuated iNOS expression in BMDMs, both in the presence and absence of LPS and IFNγ (Supplementary Fig. S4c, d). Taken together, these data indicate that Par3L induces M1 macrophage polarization in vitro.

Par3L activates p65 and ERK rather than p38 and JNK signaling

The mammalian Rel/NF-κB family members, including p50, p52, p65, RelB, and c-Rel subunits, play a pivotal role in inflammation and metabolic disease [39]. MAPK is an evolutionarily highly conserved group of serine-threonine kinases mainly comprising four subfamilies: ERK, p38, JNK, and BMK1 [40–42], which play a critical role in cardiovascular disease [10, 43]. Notably, activation of the NF-κB p65 subunit modulates M1 polarization through TLR ligands to produce pro-inflammatory factors [44]. The 1, 2-ethylenediamine SQ109 promotes M1 macrophage polarization through the p38 MAPK pathway [45]. Given the critical roles of NF-κB and MAPK in M1 macrophage polarization [46–48], we sought to determine whether Par3L affects these pathways. As shown in Fig. 6a–d, the results show that Par3L overexpression increased p-p65 and p-ERK1/2 in PMs treated with LPS and IFNγ for 30 min, as indicated. However, no significant changes in p-p38 and p-JNK were observed in PMs infected with either Ad-GFP or Ad-hPar3L (Fig. 6e–h). Taken together, these data reveal that Par3L overexpression induces M1 macrophage polarization by activating p65 and ERK signaling.

Inhibition of the NF-κB and ERK signaling reverses Par3L-induced M1 macrophage polarization

We finally asked whether the inhibition NF-κB or ERK could eliminate the effects of Par3L on M1 macrophage polarization. To this end, PMs were infected with Ad-GFP or Ad-hPar3L for 24 h, and then pretreated with or without 5 μM NF-κB inhibitor Bay 11-7082 or 10 μM ERK inhibitor PD98059 for 30 min, and then stimulated with LPS (100 ng/mL) and IFNγ (20 ng/mL) for 24 h. These data indicated that Bay 11-7082 and PD98059 markedly suppressed the protein expression levels of iNOS, ArgII, pro-IL-1β, and cleaved IL-1β in PMs compared with Ad-hPar3L groups (Fig. 7a–d). Taken together, these data demonstrate that blocking NF-κB and ERK signaling abolishes the effect of Par3L on M1 macrophage polarization.

DISCUSSION

Here, we unveiled a novel role of the Par3-like polarity protein Par3L in the pathogenesis of atherosclerosis. First, we observed increased Par3L expression in human and mouse atherosclerotic plaques and ox-LDL-treated mouse primary macrophages. Second, we showed that adenovirus-mediated Par3L overexpression accelerated atherosclerosis and induced M1 macrophage polarization in *Apoe*$^{-/-}$ mice. Third, we dissected that Par3L overexpression promoted macrophage polarization to M1 phenotype by activating LPS and IFNγ-induced p65 and ERK signaling, which can be suppressed by NF-κB inhibitor Bay 11-7082 and ERK inhibitor PD98059 in vitro (Fig. 8). These findings suggest that inhibiting Par3L could serve as an effective strategy for treating atherosclerosis.

Cell polarity is fundamental for several essential life activities, such as cell development, cell differentiation, and cell proliferation [49]. Loss of cell polarity is a hallmark of cancer and inflammatory diseases [50, 51]. Proteins involved in the cell apico-lateral polarization include the Par complex (Par3/Par6/aPKC), Crumbs (Crumbs/Pals1/Patj) complex, and Scribble complex (Scrib, Lgl, and Dlg) [52]. Par3L, also known as Pard3B, Par3B, or Par3β, is a novel homolog of the Par3 family first described in 2002 [19, 20]. Par3L is widely distributed in various tissues, including the kidney, heart, lung, skeletal muscle, and liver [19, 20]. Previous studies have shown that the testosterone AR-Par3L signaling axis promotes human glioblastoma multiforme (GBM) tumorigenesis and cell proliferation [53]. The expression level of Par3L was increased during differentiation in immortalized mouse podocytes [54]. However, podocyte-specific Par3B knockout does not cause glomerular disease phenotype and Par3A/B double-knockout mice show severe glomerular dysfunction [55]. Recently, a genome-wide association study (GWAS) using the UK Biobank showed that PARD3B rs188937806 is positively associated with hypertrophic cardiomyopathy (HCM) [56], indicating a potential role of Par3L in the pathogenesis of the cardiovascular disease. We demonstrated here that Par3L was upregulated in the macrophages of human and mouse atherosclerotic plaques and could be induced by an independent risk factor oxLDL in macrophages in vitro. By overexpressing Par3L via adenovirus, we found that Par3L aggravated atherosclerosis and macrophage inflammation. In contrast, the polarity protein Scrib (Scribble 1) has been shown to play an atheroprotective role by interacting with Arhgef7 (Rho Guanine Nucleotide Exchange Factor 7, βPix) to maintain endothelial cell function [52]. The functions of Par3L in migration, cell division, and tumor cell metastasis have been well-documented in tumor research. However, Par3L, a polarity protein, and its involvement in M1 macrophage polarization and atherosclerotic formation have remained elusive. In our study, we have made significant progress by providing the first evidence of the

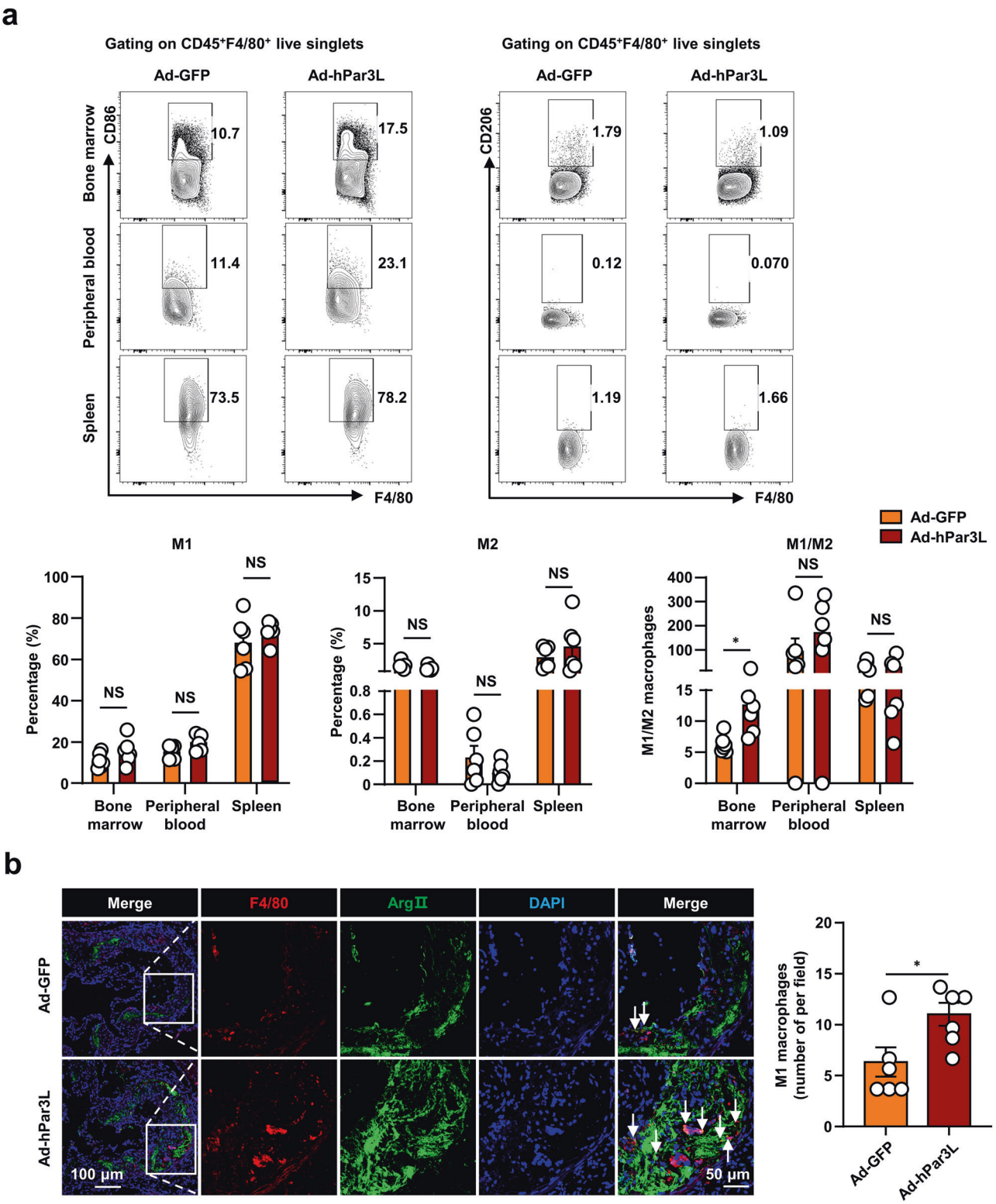

Fig. 4 Adenovirus-mediated Par3L overexpression regulates M1 macrophage polarization in *Apoe*$^{-/-}$ mice in vivo. Flow cytometry analyzed the bone marrow, peripheral blood, and spleen of *Apoe*$^{-/-}$ mice injected with Ad-GFP or Ad-hPar3L. **a** Representative plots and percentages of M1 macrophages (F4/80^{+}CD86^{+}) and M2 macrophages (F4/80^{+}CD206^{+}) among CD45^{+}F4/80^{+} cells were shown ($n = 6$ mice). The ratio of M1 to M2 macrophages was calculated ($n = 6$ mice). **b** Immunofluorescence images of atherosclerotic lesions double-stained with F4/80 and ArgII. Quantification of double-positive cells (F4/80^{+}ArgII^{+}) in aortic root sections, as shown by white arrows ($n = 6$ mice). Scale bar = 50 or 100 μm. Data are presented as mean ± SEM. *P* values were determined using unpaired, two-tailed Student's *t*-test. NS not significant. $^{*}P < 0.05$, significantly different as indicated.

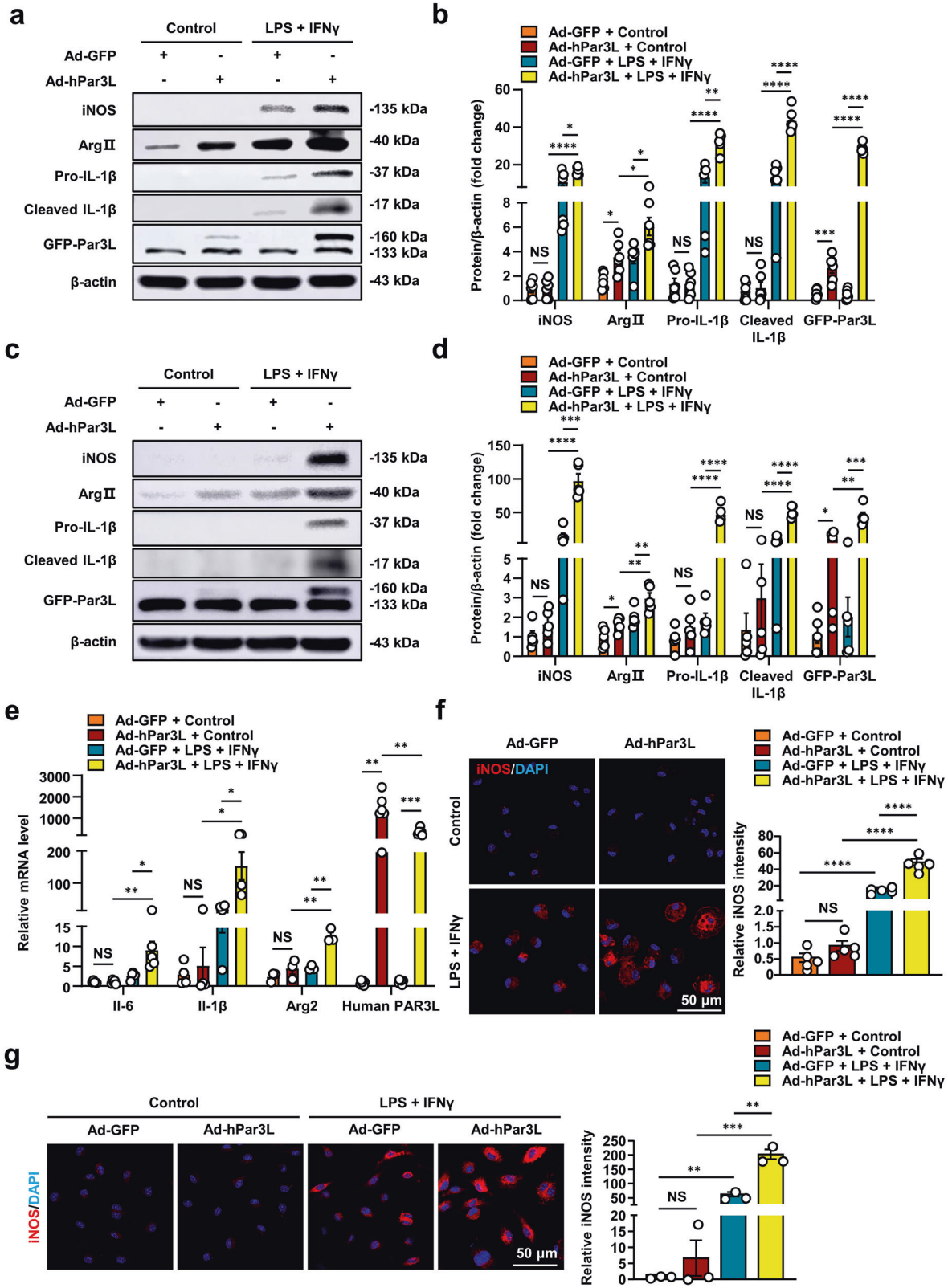

Fig. 5 Par3L promotes LPS and IFNγ-induced M1 macrophage polarization in vitro. BMDMs or PMs were infected with Ad-GFP or Ad-hPar3L for 24 h and then treated with or without LPS (100 ng/mL) and IFNγ (20 ng/mL) for 24 h. **a**, **b** Representative immunoblots and quantification of iNOS, ArgII, pro-IL-1β, cleaved IL-1β, and GFP-Par3L in BMDMs ($n = 6$). β-actin served as an internal control. **c**, **d** Representative immunoblots and quantification of iNOS, ArgII, pro-IL-1β, cleaved IL-1β, and GFP-Par3L in PMs ($n = 5$). β-actin served as an internal control. **e** qPCR analysis of *Il-6*, *Il-1β*, *Arg2* and *human PAR3L* mRNA levels in PMs ($n = 3$ or 6). *Gapdh* served as an internal control. **f** Representative images of iNOS immunofluorescent staining in PMs ($n = 5$). Scale bar = 50 μm. **g** Representative images of iNOS immunofluorescent staining in BMDMs ($n = 3$). Scale bar = 50 μm. Data are presented as mean ± SEM. *P* values were determined using unpaired, two-tailed Student's *t*-test. NS, not significant. $^{*}P < 0.05$, $^{**}P < 0.01$, $^{***}P < 0.001$ and $^{****}P < 0.0001$, significantly different as indicated.

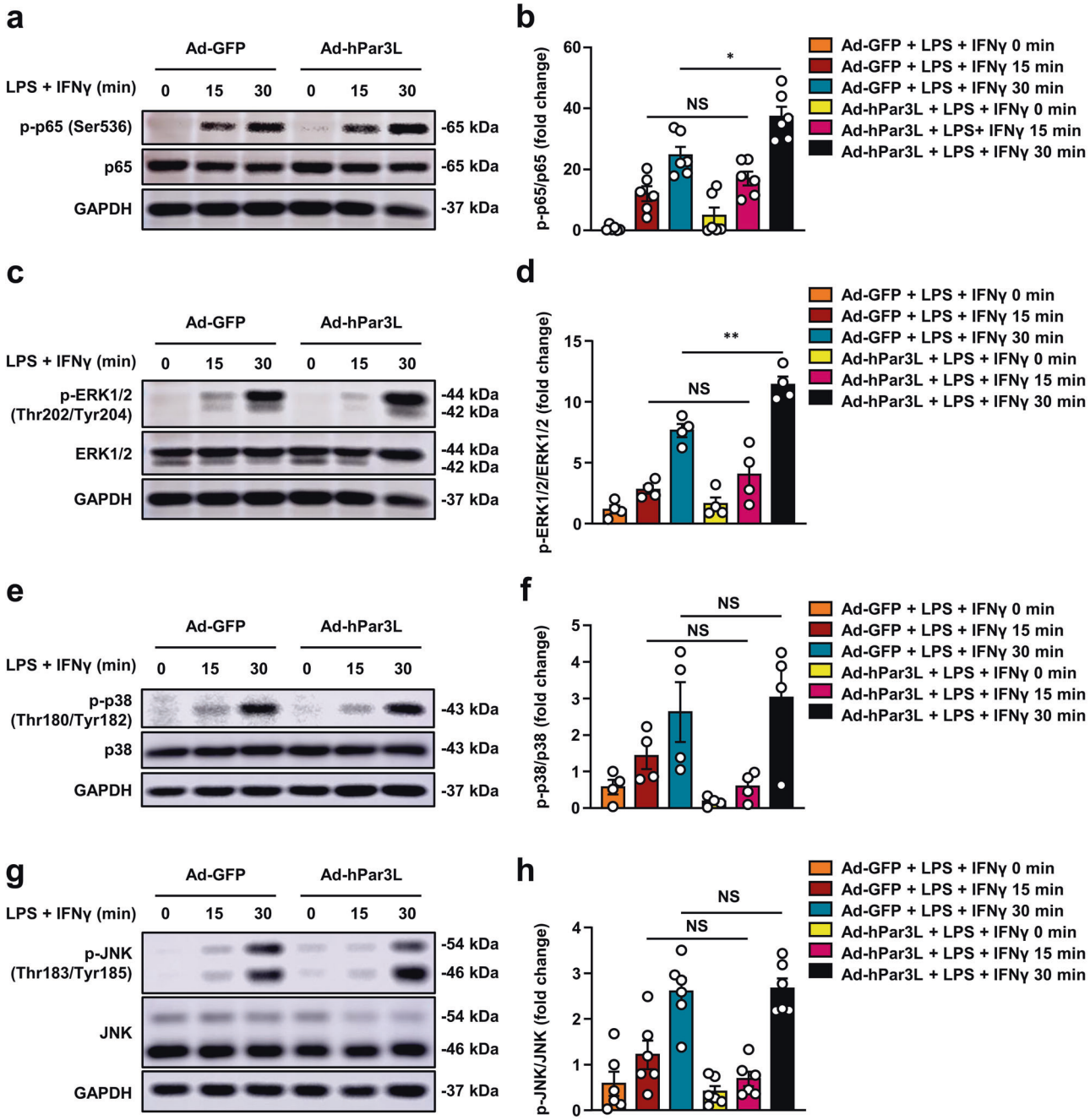

Fig. 6 Par3L increases the phosphorylation of p65 and ERK1/2 rather than p38 and JNK. PMs were infected with Ad-GFP or Ad-hPar3L for 48 h and then treated with or without LPS (100 ng/mL) and IFNγ (20 ng/mL) for 0 min, 15 min, or 30 min. **a**, **b** Representative immunoblots and quantification of p-p65 (Ser536) and p65 in PMs ($n = 6$). GAPDH served as an internal control. **c**, **d** Representative immunoblots and quantification of p-ERK1/2 (Thr202/Tyr204) and ERK1/2 in PMs ($n = 4$). GAPDH served as an internal control. **e**, **f** Representative immunoblots and quantification of p-p38 (Thr180/Tyr182) and p38 protein levels in PMs ($n = 4$). GAPDH served as an internal control. **g**, **h** Representative immunoblots and quantification of p-JNK (Thr183/Tyr185) and JNK in PMs ($n = 6$). GAPDH served as an internal control. Data are presented as mean ± SEM. *P* values were determined using unpaired, two-tailed Student's *t*-test. NS not significant. $^{*}P < 0.05$, $^{**}P < 0.01$, significantly different as indicated.

role played by Par3L in exacerbating atherosclerosis and promoting M1 macrophage polarization. Therefore, our findings contribute to advancing the understanding of polarity protein biology and its implications in pathological conditions.

Macrophages are immune cells actively involved in all the stages of atherosclerosis development. Circulating macrophages infiltrate into the subintimal space of medium and large arteries. Infiltrated macrophages can either be induced to polarize to pro-inflammatory M1 macrophages by LPS and IFNγ or anti-inflammatory M2 macrophages by IL-4 and IL-13. M1 macrophages secrete pro-inflammatory cytokines and chemokines, which recruit more monocytes to the lesion area and contribute to vascular inflammation and atherosclerosis [57]. Recent studies have found that regulating macrophage polarization may represent a promising strategy to suppress atherosclerosis. For example, inhibition of miR-494-3p reduces atherosclerotic plaque formation by activating Wnt signaling to inhibit M1 polarization and increase M2 polarization [15]. Artesunate (ART) exerts

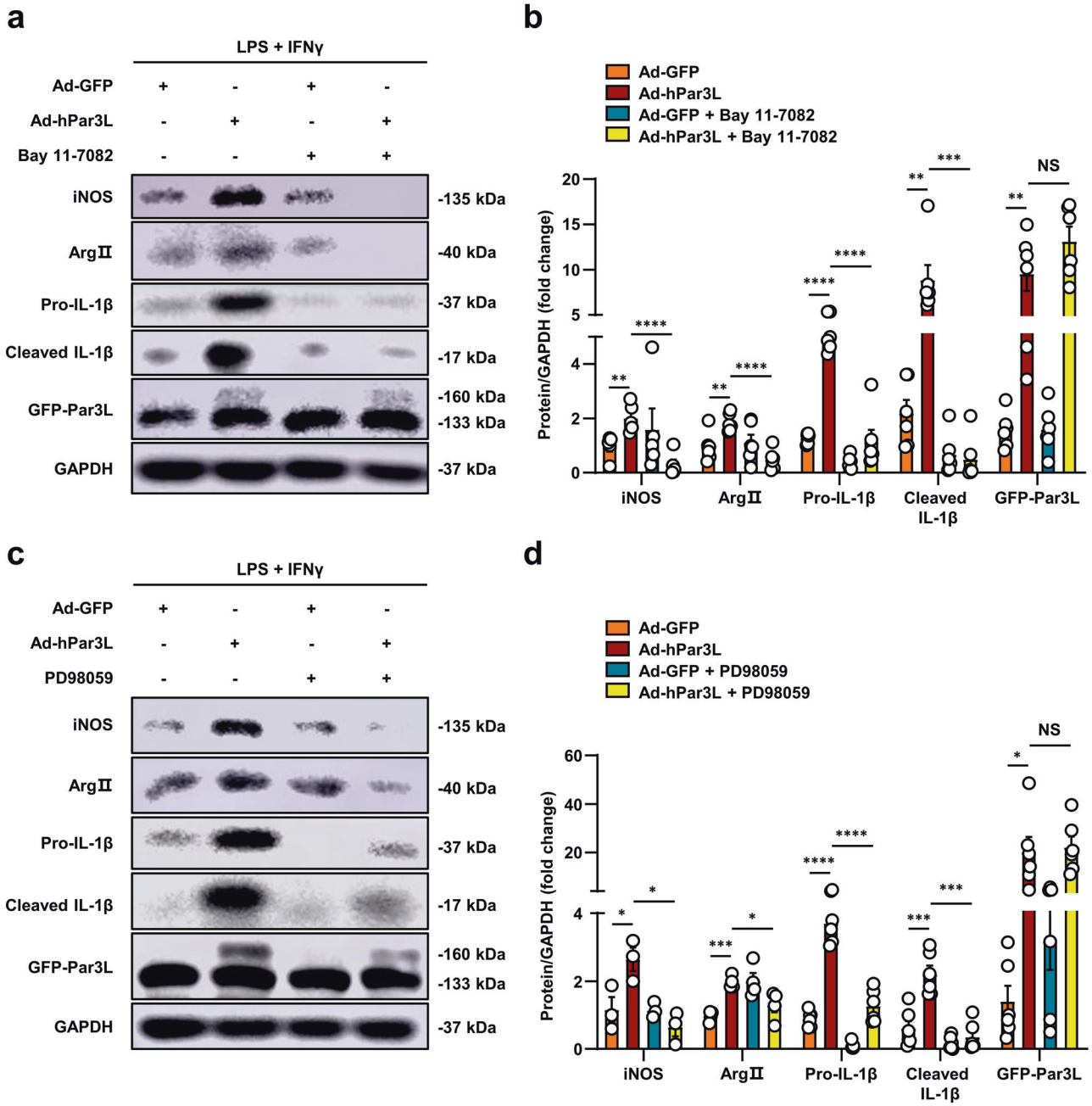

Fig. 7 Inhibiting NF-κB or ERK signaling reverses Par3L-mediated M1 macrophage polarization. PMs were infected with Ad-GFP or Ad-hPar3L for 24 h, and then treated with or without 5 μM NF-κB inhibitor Bay 11-7082 (**a**, **b**) or 10 μM ERK inhibitor PD98059 (**c**, **d**) for 30 min, followed by LPS (100 ng/mL) and IFNγ (20 ng/mL) stimulation for 24 h. **a–d** Representative immunoblots and quantification of iNOS, ArgII, pro-IL-1β, cleaved IL-1β, and GFP-Par3L in PMs ($n = 3$ or 6). GAPDH served as an internal control. Data are presented as mean ± SEM. *P* values were determined using unpaired, two-tailed Student's *t*-test. NS not significant. $^{*}P < 0.05$, $^{**}P < 0.01$, $^{***}P < 0.001$ and $^{****}P < 0.0001$, significantly different as indicated.

anti-atherosclerosis effects by inhibiting M1 polarization via regulating HIF-1α and NF-κB signaling pathways [58]. Ginsenoside Rb2 (Rb2) attenuates atherosclerotic plaque lesions and inhibits M1 macrophage polarization by targeting miR-216a [16]. Myeloid-specific CD40-deficient against atherosclerosis by suppressing M1 macrophage polarization [59]. We demonstrated for the first time that Par3L promoted LPS and IFNγ-induced M1 macrophage polarization in vitro. NF-κB and MAPK pathways can induce M1 macrophage polarization [57]. We observed increased phosphorylation of p65 and ERK1/2 in Par3L-overexpressed macrophages. Notably, NF-κB inhibitor Bay 11-7082 or ERK inhibitor PD98059 drastically reversed the effect of Par3L on M1 macrophage polarization.

Another interesting observation is that adenovirus-mediated Par3L overexpression increased non-HDL-C levels and decreased HDL-C levels in the plasma of Western diet-fed *Apoe*$^{-/-}$ mice. The liver is closely related to lipid metabolism. Hepatic cholesterol transport is key in Western diet-induced atherosclerosis in *Apoe*$^{-/-}$ mice [60]. Recent studies have shown that regulating the expression of hepatic cyclic AMP-responsive element-binding protein H (CREBH), a key regulator of lipid and glucose metabolism as well as inflammation, can prevent atherosclerosis [61]. We found that

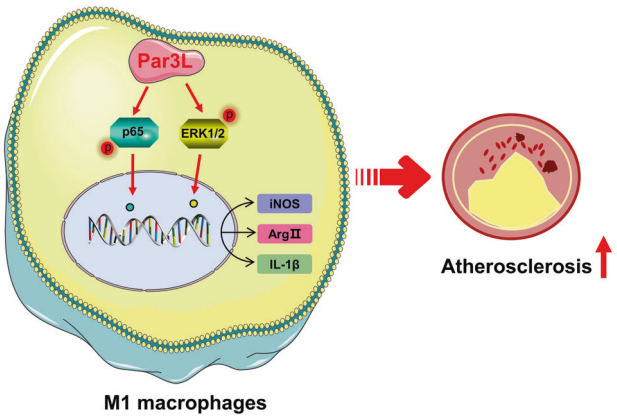

Fig. 8 Model for the role of Par3L in macrophage M1 polarization and atherosclerosis. Par3L induces macrophage polarization toward M1 phenotypes through p65 and ERK activation, aggravating atherosclerosis in *Apoe*$^{-/-}$ mice.

Par3L overexpression increased the expression of *Cebpa* in the liver of *Apoe*$^{-/-}$ mice. However, no significant difference was observed in *Pparg*, *Atgl*, *Fabp4*, *Lpl*, *Fasn*, *Srebp-1c*, and *Accb* mRNA levels. Altogether, these results indicated that Par3L might affect plasma lipid and atherosclerosis in *Apoe*$^{-/-}$ mice by increasing the expression of *Cebpa*, a critical transcription factor that affects lipid and cholesterol metabolism [62].

We realized that this study has some limitations. Although we uncovered a role of Par3L in M1 macrophage polarization, we did not know whether Par3L affects M2 macrophage polarization. Moreover, to dissect the exact role of macrophage Par3L in atherosclerosis, myeloid cell-specific Par3L knockout mice on *Apoe*$^{-/-}$ background mice need to be generated. Finally, the underlying mechanism by which Par3L regulates *Cebpa* expression warrants further investigation.

In conclusion, we demonstrated that Par3L induces macrophage M1 polarization and aggravates atherosclerosis by activating the NF-κB and ERK pathways. Our study identifies Par3L as a crucial endogenous regulator for M1 macrophage polarization and a promising therapeutic target for ASCVD.

ACKNOWLEDGEMENTS

This work was supported in part by the National Natural Science Foundation of China (81974046 and 82170467), the Natural Science Foundation of Guangdong (2022A1515012502), and the Sixth Affiliated Hospital of Guangzhou Medical University, Qingyuan People's Hospital (202201-301), and Discipline Development Project of Guangzhou Medical University, China (02-445-2301221XM).

AUTHOR CONTRIBUTIONS

XYD directed the project, designed the experiments, and revised the manuscript. YMH performed experiments, analyzed and interpreted the data, and drafted the manuscript. KYM and YSW performed experiments and analyzed data. YYD and YMX supervised the experiments. All authors read the final manuscript.

ADDITIONAL INFORMATION

Supplementary information The online version contains supplementary material available at https://doi.org/10.1038/s41401-023-01161-z.

Competing interests: The authors declare no competing interests.

REFERENCES

1. Tsao CW, Aday AW, Almarzooq ZI, Alonso A, Beaton AZ, Bittencourt MS, et al. Heart disease and stroke statistics-2022 update: a report from the American Heart Association. Circulation. 2022;145:e153–e639.
2. Hansson GK. Inflammation, atherosclerosis, and coronary artery disease. N Engl J Med. 2005;352:1685–95.
3. Hansson GK, Hermansson A. The immune system in atherosclerosis. Nat Immunol. 2011;12:204–12.
4. Barrett TJ. Macrophages in atherosclerosis regression. Arterioscler Thromb Vasc Biol. 2020;40:20–33.
5. Moore KJ, Sheedy FJ, Fisher EA. Macrophages in atherosclerosis: a dynamic balance. Nat Rev Immunol. 2013;13:709–21.
6. Colin S, Chinetti-Gbaguidi G, Staels B. Macrophage phenotypes in atherosclerosis. Immunol Rev. 2014;262:153–66.
7. Mosser DM, Edwards JP. Exploring the full spectrum of macrophage activation. Nat Rev Immunol. 2008;8:958–69.
8. Tabas I, Bornfeldt KE. Macrophage phenotype and function in different stages of atherosclerosis. Circ Res. 2016;118:653–67.
9. Haftcheshmeh SM, Abedi M, Mashayekhi K, Mousavi MJ, Navashenaq JG, Mohammadi A, et al. Berberine as a natural modulator of inflammatory signaling pathways in the immune system: focus on NF-kappaB, JAK/STAT, and MAPK signaling pathways. Phytother Res. 2022;36:1216–30.
10. Karimian MS, Pirro M, Majeed M, Sahebkar A. Curcumin as a natural regulator of monocyte chemoattractant protein-1. Cytokine Growth Factor Rev. 2017;33:55–63.
11. Yu G, Yu H, Yang Q, Wang J, Fan H, Liu G, et al. Vibrio harveyi infections induce production of proinflammatory cytokines in murine peritoneal macrophages via activation of p38 MAPK and NF-kappaB pathways, but reversed by PI3K/AKT pathways. Dev Comp Immunol. 2022;127:104292.
12. Wang LX, Zhang SX, Wu HJ, Rong XL, Guo J. M2b macrophage polarization and its roles in diseases. J Leukoc Biol. 2019;106:345–58.
13. Verreck FA, de Boer T, Langenberg DM, Hoeve MA, Kramer M, Vaisberg E, et al. Human IL-23-producing type 1 macrophages promote but IL-10-producing type 2 macrophages subvert immunity to (myco)bacteria. Proc Natl Acad Sci USA. 2004;101:4560–5.
14. Ridker PM, Luscher TF. Anti-inflammatory therapies for cardiovascular disease. Eur Heart J. 2014;35:1782–91.
15. van Ingen E, Foks AC, Woudenberg T, van der Bent ML, de Jong A, Hohensinner PJ, et al. Inhibition of microRNA-494-3p activates Wnt signaling and reduces proinflammatory macrophage polarization in atherosclerosis. Mol Ther Nucleic Acids. 2021;26:1228–39.
16. Wang S, Yang S, Chen Y, Chen Y, Li R, Han S, et al. Ginsenoside Rb2 alleviated atherosclerosis by inhibiting M1 macrophages polarization induced by microRNA-216a. Front Pharmacol. 2021;12:764130.
17. Zhang X, Li J, Luo S, Wang M, Huang Q, Deng Z, et al. IgE Contributes to atherosclerosis and obesity by affecting macrophage polarization, macrophage protein network, and foam cell formation. Arterioscler Thromb Vasc Biol. 2020;40:597–610.
18. Li T, Ding L, Wang Y, Yang O, Wang S, Kong J. Genetic deficiency of Phactr1 promotes atherosclerosis development via facilitating M1 macrophage polarization and foam cell formation. Clin Sci. 2020;134:2353–68.
19. Gao L, Macara IG, Joberty G. Multiple splice variants of Par3 and of a novel related gene, Par3L, produce proteins with different binding properties. Gene. 2002;294:99–107.
20. Kohjima M, Noda Y, Takeya R, Saito N, Takeuchi K, Sumimoto H. PAR3beta, a novel homologue of the cell polarity protein PAR3, localizes to tight junctions. Biochem Biophys Res Commun. 2002;299:641–6.
21. Izaki T, Kamakura S, Kohjima M, Sumimoto H. Phosphorylation-dependent binding of 14-3-3 to Par3beta, a human Par3-related cell polarity protein. Biochem Biophys Res Commun. 2005;329:211–8.
22. Thompson BJ. Par-3 family proteins in cell polarity & adhesion. FEBS J. 2022;289:596–613.
23. Huo Y, Macara IG. The Par3-like polarity protein Par3L is essential for mammary stem cell maintenance. Nat Cell Biol. 2014;16:529–37.
24. Li T, Liu D, Lei X, Jiang Q. Par3L enhances colorectal cancer cell survival by inhibiting Lkb1/AMPK signaling pathway. Biochem Biophys Res Commun. 2017;482:1037–41.
25. Dai X, Ding Y, Liu Z, Zhang W, Zou MH. Phosphorylation of CHOP (C/EBP Homologous Protein) by the AMP-Activated protein kinase alpha 1 in macrophages promotes CHOP degradation and reduces injury-induced neointimal disruption in vivo. Circ Res. 2016;119:1089–1100.
26. Ray A, Dittel BN. Isolation of mouse peritoneal cavity cells. J Vis Exp. 2010;28:1488.
27. Geng T, Yan Y, Xu L, Cao M, Xu Y, Pu J, et al. CD137 signaling induces macrophage M2 polarization in atherosclerosis through STAT6/PPARdelta pathway. Cell Signal. 2020;72:109628.
28. Huang Y, Ma K, Qin R, Fang Y, Zhou J, Dai X. Pristane attenuates atherosclerosis in Apoe(-/-) mice via IL-4-secreting regulatory plasma cell-mediated M2 macrophage polarization. Biomed Pharmacother. 2022;155:113750.

29. Ma C, Xia R, Yang S, Liu L, Zhang J, Feng K, et al. Formononetin attenuates atherosclerosis via regulating interaction between KLF4 and SRA in apoE(-/-) mice. Theranostics. 2020;10:1090–106.
30. Wen B, Dang YY, Wu SH, Huang YM, Ma KY, Xu YM, et al. Antiatherosclerotic effect of dehydrocorydaline on ApoE(-/-) mice: inhibition of macrophage inflammation. Acta Pharmacol Sin. 2022;43:1408–18.
31. Williams H, Johnson JL, Carson KG, Jackson CL. Characteristics of intact and ruptured atherosclerotic plaques in brachiocephalic arteries of apolipoprotein E knockout mice. Arterioscler Thromb Vasc Biol. 2002;22:788–92.
32. Tie L, Xiao H, Wu DL, Yang Y, Wang P. A brief guide to good practices in pharmacological experiments: Western blotting. Acta Pharmacol Sin. 2021;42:1015–7.
33. Kopin L, Lowenstein C. Dyslipidemia. Ann Intern Med. 2017;167:ITC81–ITC96.
34. Gomez-Delgado F, Katsiki N, Lopez-Miranda J, Perez-Martinez P. Dietary habits, lipoprotein metabolism and cardiovascular disease: from individual foods to dietary patterns. Crit Rev Food Sci Nutr. 2021;61:1651–69.
35. Casula M, Colpani O, Xie S, Catapano AL, Baragetti A. HDL in atherosclerotic cardiovascular disease: in search of a role. Cells. 2021;10:1869.
36. Seebacher F, Zeigerer A, Kory N, Krahmer N. Hepatic lipid droplet homeostasis and fatty liver disease. Semin Cell Dev Biol. 2020;108:72–81.
37. Alves-Bezerra M, Cohen DE. Triglyceride metabolism in the liver. Compr Physiol. 2017;8:1–8.
38. Watt MJ, Miotto PM, De Nardo W, Montgomery MK. The liver as an endocrine organ-linking NAFLD and insulin resistance. Endocr Rev. 2019;40:1367–93.
39. Baker RG, Hayden MS, Ghosh S. NF-kappaB, inflammation, and metabolic disease. Cell Metab. 2011;13:11–22.
40. Yoshizumi M, Kyotani Y, Zhao J, Nagayama K, Ito S, Tsuji Y, et al. Role of big mitogen-activated protein kinase 1 (BMK1)/extracellular signal-regulated kinase 5 (ERK5) in the pathogenesis and progression of atherosclerosis. J Pharm Sci. 2012;120:259–63.
41. Tubita A, Lombardi Z, Tusa I, Dello Sbarba P, Rovida E. Beyond kinase activity: ERK5 nucleo-cytoplasmic shuttling as a novel target for anticancer therapy. Int J Mol Sci. 2020;21:938.
42. Kim HS, Asmis R. Mitogen-activated protein kinase phosphatase 1 (MKP-1) in macrophage biology and cardiovascular disease. A redox-regulated master controller of monocyte function and macrophage phenotype. Free Radic Biol Med. 2017;109:75–83.
43. Muslin AJ. MAPK signalling in cardiovascular health and disease: molecular mechanisms and therapeutic targets. Clin Sci. 2008;115:203–18.
44. Bonizzi G, Karin M. The two NF-kappaB activation pathways and their role in innate and adaptive immunity. Trends Immunol. 2004;25:280–8.
45. Singh M, Kumar S, Singh B, Jain P, Kumari A, Pahuja I, et al. The 1, 2-ethylenediamine SQ109 protects against tuberculosis by promoting M1 macrophage polarization through the p38 MAPK pathway. Commun Biol. 2022;5:759.
46. Chen XS, Wang SH, Liu CY, Gao YL, Meng XL, Wei W, et al. Losartan attenuates sepsis-induced cardiomyopathy by regulating macrophage polarization via TLR4-mediated NF-kappaB and MAPK signaling. Pharmacol Res. 2022;185:106473.
47. Ge G, Bai J, Wang Q, Liang X, Tao H, Chen H, et al. Punicalagin ameliorates collagen-induced arthritis by downregulating M1 macrophage and pyroptosis via NF-kappaB signaling pathway. Sci China Life Sci. 2022;65:588–603.
48. Fang J, Ou Q, Wu B, Li S, Wu M, Qiu J, et al. TcpC inhibits M1 but promotes M2 macrophage polarization via regulation of the MAPK/NF-kappaB and Akt/STAT6 pathways in urinary tract infection. Cells. 2022;11:2674.
49. Allam AH, Charnley M, Russell SM. Context-specific mechanisms of cell polarity regulation. J Mol Biol. 2018;430:3457–71.
50. Ellenbroek SI, Iden S, Collard JG. Cell polarity proteins and cancer. Semin Cancer Biol. 2012;22:208–15.
51. Shaha S, Patel K, Riddell M. Cell polarity signaling in the regulation of syncytiotrophoblast homeostasis and inflammatory response. Placenta. 2022:S0143-4004(22)00457-X.
52. Schurmann C, Dienst FL, Palfi K, Vasconez AE, Oo JA, Wang S, et al. The polarity protein Scrib limits atherosclerosis development in mice. Cardiovasc Res. 2019;115:1963–74.
53. Yang JD, Chen JT, Liu SH, Chen RM. Contribution of the testosterone androgen receptor-PARD3B signaling axis to tumorigenesis and malignance of glioblastoma multiforme through stimulating cell proliferation and colony formation. J Clin Med. 2022;11:4818.
54. Koehler S, Tellkamp F, Niessen CM, Bloch W, Kerjaschki D, Schermer B, et al. Par3A is dispensable for the function of the glomerular filtration barrier of the kidney. Am J Physiol Ren Physiol. 2016;311:F112–119.
55. Koehler S, Odenthal J, Ludwig V, Unnersjo Jess D, Hohne M, Jungst C, et al. Scaffold polarity proteins Par3A and Par3B share redundant functions while Par3B acts independent of atypical protein kinase C/Par6 in podocytes to maintain the kidney filtration barrier. Kidney Int. 2022;101:733–51.
56. Gyftopoulos A, Chen YJ, Wang L, Williams CH, Chun YW, O'Connell JR, et al. Identification of novel genetic variants and comorbidities associated with ICD-10-based diagnosis of hypertrophic cardiomyopathy using the UK Biobank Cohort. Front Genet. 2022;13:866042.
57. Blagov AV, Markin AM, Bogatyreva AI, Tolstik TV, Sukhorukov VN, Orekhov AN. The role of macrophages in the pathogenesis of atherosclerosis. Cells. 2023;12:522.
58. Wang X, Du H, Li X. Artesunate attenuates atherosclerosis by inhibiting macrophage M1-like polarization and improving metabolism. Int Immunopharmacol. 2022;102:108413.
59. Bosmans LA, van Tiel CM, Aarts S, Willemsen L, Baardman J, van Os BW, et al. Myeloid CD40 deficiency reduces atherosclerosis by impairing macrophages' transition into a pro-inflammatory state. Cardiovasc Res. 2023;119:1146–60.
60. Li H, Yu XH, Ou X, Ouyang XP, Tang CK. Hepatic cholesterol transport and its role in non-alcoholic fatty liver disease and atherosclerosis. Prog Lipid Res. 2021;83:101109.
61. Attie AD. Recruiting a transcription factor in the liver to prevent atherosclerosis. J Clin Invest. 2021;131:e154677.
62. Danielewski M, Matuszewska A, Szelag A, Sozanski T. The impact of anthocyanins and iridoids on transcription factors crucial for lipid and cholesterol homeostasis. Int J Mol Sci. 2021;22:6074.